Magnetoplasmon resonances in polycrystalline bismuth as seen via time-domain terahertz spectroscopy

Julien Levallois,[*] Piotr Chudziński,[†] Jason N. Hancock,[‡] Alexey B. Kuzmenko, and Dirk van der Marel
Département de Physique de la Matière Condensée, Université de Genève, CH-1211 Genève 4, Switzerland
(Received 3 September 2013; revised manuscript received 23 January 2014; published 17 April 2014)

We report the magnetic-field-dependent far-infrared reflectivity of polycrystalline bismuth. We observe four distinct absorptions that we attribute to magnetoplasmon resonances, which are collective modes of an electron-hole liquid in a magnetic field and become optical and acoustic resonances of the electron-hole system in the small-field limit. Acoustic mode are only when the masses of distinct components are very different, which is the case in bismuth. In a polycrystal, where the translational symmetry is broken, a big shift of spectral weight to an acoustic plasmon is possible. This enables us to detect an associated plasma edge. Although the polycrystal sample has grains of randomly distributed orientations, our reflectivity results can be explained by invoking only two, clearly distinct, series of resonances. In the limit of zero field, the optical modes of these two series converge onto plasma frequencies measured in a monocrystal along the main optical axes.

DOI: 10.1103/PhysRevB.89.155123 PACS number(s): 78.30.Er, 71.45.Gm, 78.20.Ls

I. INTRODUCTION

Pure bismuth exhibits rich physics due to its particular electronic properties. In its pristine state, it is an exactly charge-compensated semimetal of electrons and holes. Peculiar to bismuth is the low carrier density ($\sim 10^{17}$ cm^{-3}) and extremely anisotropic cyclotron masses [1]. Magneto-oscillation phenomena are therefore easily accessible and in fact were discovered in bismuth [2,3]. The Fermi surface of bismuth, which is depicted in Fig. 1, is highly anisotropic and made by three elongated ellipsoid (Dirac) electron pockets, which are slightly tilted by 6° from the bisectrix axis (C_1), and one ellispoidal hole (massive) pocket along the trigonal axis (C_3) [4], each having a volume that represents only a few percent of the Brillouin zone. This material is of central interest because it is a key player of high-T_c superconductors, it has been found to host a transition to a topological insulating state by partial substitution with isoelectronic antimony [5], and it is promising for valley-tronics [6]. The observations of a valley-ferromagnetic state [7] and optical evidence for electron-plasmon coupling [8] have led to a revival of interest in the collective excitations and low-temperature transport properties of this material [9].

The extremely large ratio of masses of different carriers has one highly nontrivial implication: the presence of an additional collective excitation of a Fermi liquid, which manifests as an acoustic resonance. Its existence in two-component plasmas was already suggested a long time ago [10], but direct detection of this collective mode turned out to be quite elusive. In particular, from the viewpoint of optical spectroscopy there are two fundamental obstacles. First, when $q \to 0$, which is the usual resonance condition with photons, the energy of an acoustic plasmon vanishes. This issue can be solved by applying a magnetic field because the movement of a charge under a magnetic field requires extra kinetic energy to overcome the magnetic vector potential. The resonance frequency becomes $\omega = \sqrt{\omega_p^2 + \omega_c^2}$, where ω_p and ω_c are the screened plasma and the cyclotron frequency, respectively. Such a simple addition formula works due to Kohn's theorem and has been shown to work in numerous studies: from a semiclassical approximation for a dielectric tensor [11] or a self-consistent field [12], later with an equation-of-motion technique [13], and finally using polarizabilities known from the random-phase approximation (RPA) polarizability [14] and recently extended by including vertex corrections to the RPA [15].

Secondly, in the case of translationally invariant systems, the longitudinal f-sum rule warrants that in the limit of small fields, $B \to 0$, the excitation proportional to the total carrier density (standard, optical plasmon) exhausts all spectral weight. This creates another serious obstacle in experimental efforts to directly observe acoustic plasmons because these low-energy collective excitations would have a noticeable spectral weight only at rather high magnetic field (for Bi above ≈ 6 T), at which point it would slowly evolve into cyclotron resonance of the heavier carriers [see Eq. (1) and discussion in Sec. IV].

The translational invariance implies that the electron wavelength is a good quantum number, which is a necessary condition in every derivation of the above-mentioned longitudinal f-sum rule. Thus, the natural way to overcome this obstacle and detect an acoustic plasmon is to work with a system with a broken translational symmetry. This is our motivation to perform a measurement on a polycrystalline bismuth.

II. EXPERIMENT

The sample used in this study is a bismuth polycrystal that consists of half of a 12 mm diameter disk and 2 mm thick. The sample was characterized by x-ray diffraction, which shows that all orientations (C_1, C_2, and C_3) are equally and randomly present with a grain size of $\sim$100 nm. We have measured the optical reflectivity at $\sim$5 K in the range

[*]julien.levallois@unige.ch
[†]Present address: Institute of Theoretical Physics, University of Regensburg, D-93040 Regensburg, Germany; Piotr.Chudzinski@physik.uni-regensburg.de
[‡]Present address: Department of Physics and Institute of Materials Science, University of Connecticut, Storrs, CT 06269, USA.

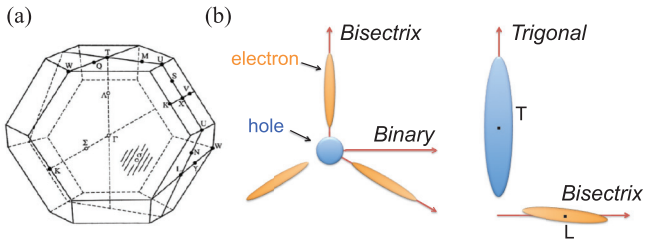

FIG. 1. (Color online) (a) The Brillouin zone with the main symmetry points (adapted from Ref. [4]). b) The Fermi surface of bismuth: a hole pocket that is an ellipsoid elongated along the trigonal axis (C_3) and three electron pockets distributed in a threefold-degenerate pocket around the C_3 axis. They are not perfectly aligned with the bisectrix axis (C_1) but tilted by 6°. The binary axis (C_2) is orthogonal to the C_1 axis.

5–650 cm^{-1} by time-domain THz spectroscopy (TPI spectra 1000, TeraView Ltd.) using a home-made (magneto)reflectivity setup to 3.4 T and by Fourier transform infrared spectroscopy to 7 T. In the latter case, the reflectivity was obtained using a gold mirror reference. For both instruments, the magnetic field was applied perpendicular to the surface of the sample (Faraday geometry) and nearly parallel to the propagation of light. The Kerr angle is defined as the rotation of the polarization plane upon a normal reflection of linearly polarized light from the surface of a sample and in this geometry. The Kerr angle was determined for each frequency separately by examining the dependence on the analyzer angle, as described in detail in Levallois *et al.* [16].

III. RESULTS

Figure 2(a) shows the reflectivity of polycrystalline bismuth at 5.7 K as a function of frequency and field. The general shape is in good agreement with that of a single crystal oriented along the trigonal axis [8]. The reflectivity exhibits a very strong field dependence, and we clearly observe four different plasma edgelike features in spectra collected at high field. As the magnetic field increases, the two features that are present at zero field, labeled ω_+^1 and ω_+^2, shift to higher frequencies. While ω_+^1 is present up to 6.5 T, ω_+^2 disappears above 2 T. At lower frequency, we observe the apparition of two other structures, labeled ω_-^1 and ω_-^2, whose positions and intensities increase with magnetic field, as shown in Figs. 2(b) and 2(c). The strength of these absorptions, which is proportional to the spectral weight of the associated bosonic modes, increases quite linearly at low magnetic field, as suggested in Ref. [9].

The four resonances are also visible at higher temperature, as shown in Fig. 2(d), where the reflectivity spectra at 50 K at various magnetic fields are presented. We can see that at 50 K the modes ω_+^1 and ω_+^2 disappear around 4 and 1 T, respectively, i.e., at lower fields than at 5 T. For these field values, these magnetoplasma modes shift above 220 cm^{-1}, which is also the lower bound of the interband optical conductivity seen in data from single crystal [8], suggesting that Landau damping is the main reason for the disappearance of the optical magnetoplasmons at high magnetic fields.

Figure 3 shows the ratio of the reflectivity in finite field divided by the reflectivity at zero field, $R(\omega,B)/R(\omega,0)$,

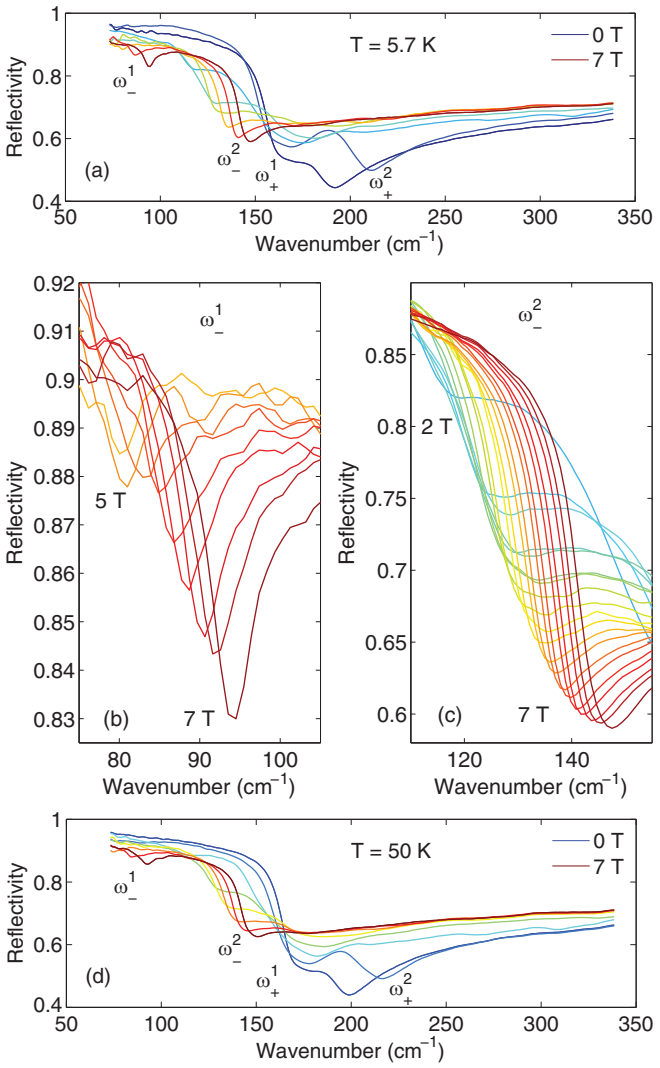

FIG. 2. (Color online) (a) Far-infrared reflectivity of polycrystalline bismuth at 5.7 K as a function of frequency at various magnetic fields (each tesla). (b) and (c) Zoom of the reflectivity around 90 cm^{-1} in order to highlight ω_-^1 and around 130 cm^{-1} in order to highlight ω_-^2, for every 0.25 T between 0 and 7 T. (d) Reflectivity at 50 K as a function of frequency at various magnetic fields (each tesla).

measured using time-domain techniques at 4.2 K up to 3.4 T. The absorption corresponding to the mode ω_-^1 is very clear. The magnetic-field dependence of the magnetoplasma frequencies of Figs. 2 and 3 is summarized in Fig. 6 for $T = 5$ and 50 K. We see that for $B \to 0$, the frequencies of the two "acoustic" modes are proportional to B.

The Kerr rotation of polycrystalline bismuth at 5.7 K is shown in Fig. 4. At low field ($B < 1.5$ T), the Kerr angle exhibits a sharp structure close to the plasma frequency, going from a negative minimum to a positive maximum. The rotation is very large even at low fields, $\theta_K \simeq 0.2$ rad at 1 T, and reaches 0.3 rad at 7 T. Moreover, it seems that the positive maximum value is linked to the plasma frequency of the second series of modes because it also disappears at 2 T. Above this field, the minimum that appears at low frequency and significantly increases in strength and shifts to higher frequency is clearly associated with the mode ω_-^2.

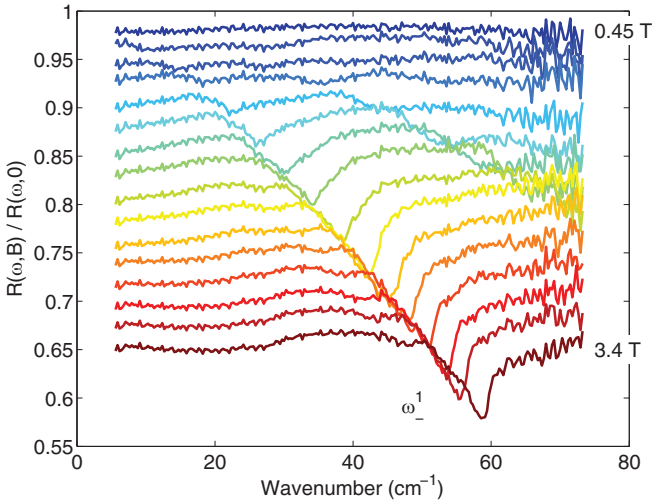

FIG. 3. (Color online) Time-domain measurement of the normal-incidence reflectivity of polycrystalline bismuth at 4.2 K at various magnetic fields. The ratio of reflectivity in finite field divided by reflectivity at zero field is plotted. Curves are shifted for clarity.

To summarize, those observations suggest that the minima and maxima of the Kerr angle are linked to light and heavy carriers, respectively. Therefore, an interpretation in terms of magnetoplasmon excitations fits the Kerr results at least qualitatively (see Sec. IV).

IV. DISCUSSION

The use of a polycrystalline samples enabled experimental observations of the modes ω_-^1 and ω_-^2 as a function of magnetic field by virtue of the fact that the grain boundaries make the optical oscillator strength for these modes finite. This advantage comes with a price, since the interpretation of the optical properties of polycrystalline materials is less straightforward than for single crystals. We start with the empirical observation that infrared reflectance spectra of polycrystals usually resemble a superposition of reflectance spectra taken with the electric field along different optical axes of the anisotropic material. In the present case, the materials should be regarded as a clustering of randomly oriented crystallites. Because the size of a monocrystal grain is much smaller than the scattered light wavelength as well as the spot size and the light penetration depth, we simultaneously measure the response of a three-dimensional (3D) set of randomly orientated grains. Since the grain boundaries provide resistive barriers for electrical transport, the appropriate theoretical model is that of a resistive network of crystallites (which can be represented by LC oscillators with plasma frequency $\omega_p = \sqrt{LC}$) connected by finite resistances representing the boundaries. The resonance frequencies of such a circuit are large and given by the plasma frequencies of the individual grains, i.e., the highest one along the trigonal axis and the lowest frequency for the two axes perpendicular to it. For brevity, we will employ here the labels a, b, and c to indicate the binary, bisectrix, and trigonal axis, respectively. Electromagnetic waves are resonantly scattered from a crystallite when the frequency matches one of the two plasma resonances, with intensity proportional to the projection of the dipole moment of plasma resonance on the electromagnetic field polarization. A related experimental work observed several plasmon branches in Bi nanoparticles [17]. There is a crucial difference with respect to our sample as in a fume the intergrain coupling is negligible.

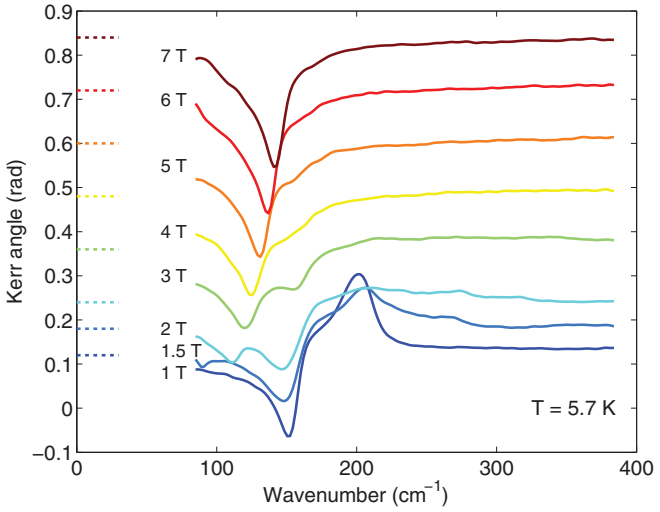

FIG. 4. (Color online) The Kerr angle spectra of polycrystalline bismuth measured at 5.7 K at various magnetic fields. The curves are shifted for clarity and the offsets are the dashed lines of the same colors.

In the data in Fig. 2(a), the minima for $B = 0$ occur at 192 and 170 cm^{-1}, i.e., very close to the minima in the reflectivity of single-crystalline bismuth [18] for the electric field polarized along the trigonal axis (187 cm^{-1}) and perpendicular to the trigonal axis (158 cm^{-1}). The Mie resonances of an individual crystallite do not exactly coincide with the bulk plasma frequencies. Factors that play a role are (i) the influence of crystallite shape, (ii) surface states, and (iii) electron energy quantization due to small crystallite size. In addition, finite coupling between crystallites affects the overall optical response. It is therefore natural to interpret the reflectance minima in Fig. 2 as the signatures of plasmons oscillating along and perpendicular to the trigonal axis.

A more quantitative microscopic description of the magnetoplasmons requires further consideration. The problem can be sketched as follows (see Fig. 5): the sample surface defines the x-y plane, and the field B is applied parallel to z. The incoming and reflected light propagates along the z axis, with the electric field in the x-y plane. The c axis of a given crystallite is tilted an angle θ with the z axis. The vacuum/grain interface is in the x-y plane, and is at an angle $\pi/2 - \theta$ with the c axis of the crystal structure. The angles α and β describe the orientation of the c axis relative to the x-y frame, and the rotation of a and b relative to the x-y-z frame. The magnetic field B induces a Lorentz force on each electron, which points to the x-y plane. By virtue of the anisotropy of the ellipsoidal electron and hole Fermi surfaces, this force depends on θ, α, and β. For $B = 0$, the solutions are plasma resonances parallel to the a-b plane and parallel to c of the individual crystallites, with frequencies close to the bulk plasma frequencies.

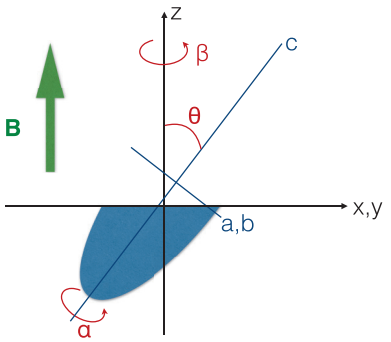

FIG. 5. (Color online) Geometry of a crystal grain (blue ellipse), truncated by the x-y plane, in order to explain our magnetoplasmon resonances (see text).

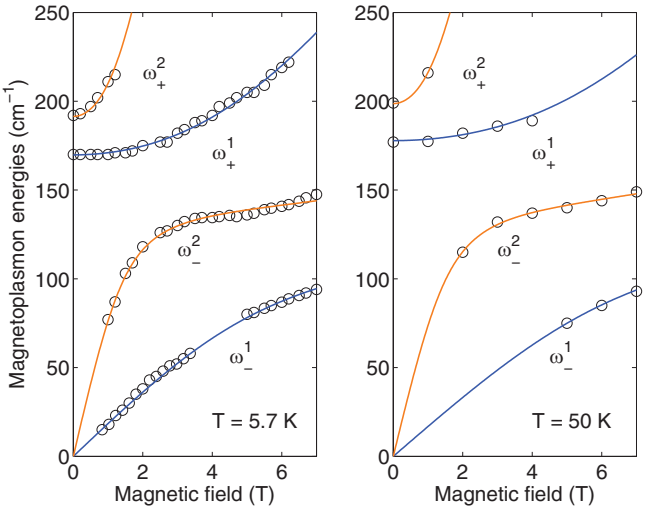

FIG. 6. (Color online) Magnetic-field dependence of the observed collective modes $\omega_\pm$ at 5.7 K (left) and at 50 K (right). Solid lines are fit from Eq. (1).

For $B \neq 0$, the situation is rather complex, and the resonance frequencies will depend on θ, α, and β as well as on B. By virtue of having both holes and electrons, acoustic and optic solutions will be found, and there will be different solutions according to the different modes of plasma oscillation. In our optical experiment, the behavior of a large ensemble of grains is observed, averaged over all grain orientations described by θ, α, and β, and taking into account the intergrain coupling. This latter is due to long-range Coulomb interactions between carriers, superposition of Mie electric fields on grain interfaces, and resistivity of intergrain boundaries. The last two in particular can introduce a substantial imaginary part to the resonance frequencies, and thus may cause overdamping of some modes (a phenomenon well known, for instance, in the Maxwell-Garnett approximation).

Although this constitutes a complicated problem, having electrons and holes causes the most striking phenomenon: as already mentioned in the Introduction, when a system consisting of two types of carriers with different cyclotron masses (heavy and light) is subjected to a perpendicular magnetic field (Faraday geometry), two magnetoplasmon edges emerge, with frequencies given by [9,14,19]

$$\omega_\pm^2 = \tfrac{1}{2}\Big[\big(\omega_{p,l}^2 + \omega_{p,h}^2 + \omega_{c,l}^2 + \omega_{c,h}^2\big) \pm \sqrt{\big(-\omega_{p,l}^2 + \omega_{p,h}^2 - \omega_{c,l}^2 + \omega_{c,h}^2\big)^2 + 4\omega_{p,l}^2\omega_{p,h}^2}\Big]. \quad (1)$$

In the limit $q \to 0$, where l and h denote light and heavy, respectively (which correspond to electrons or holes depending on the field orientation), $\omega_{p,l/h} = \sqrt{\frac{n_{l/h}e^2}{m_{l/h}\varepsilon_0\epsilon_\infty}}$ and $\omega_{c,l/h} = \frac{eB}{m_{c,l/h}}$ are the screened plasma and cyclotron frequencies, respectively, n is the density of carriers, m is the mass, ε_0 is the vacuum permittivity, and m_c is the cyclotron mass. ε_∞ accounts for the high-frequency interband transitions ($\varepsilon_\infty \simeq 100$ in Bi for $E \| ab$). This formula is obtained by resolving the equation $\varepsilon^{\mathrm{RPA}}(q \to 0, \omega) = 0$. While we are able to obtain a satisfactory dielectric tensor as a function of magnetic field [20], we find that consideration of the reflectivity minima was sufficient to understand the magnetoplasmon effects in our data. At zero field, ω_+ is merely the classical plasma frequency, equal to $\sqrt{\omega_{p,l}^2 + \omega_{p,h}^2}$. At very high magnetic fields, when the cyclotron motion dominates, these two modes $\omega_\pm$ correspond to oscillations of heavy (ω_-) and light (ω_+) carriers. In the case of bismuth, the heavier (or lighter) carrier depends on sample orientation according to the magnetic field.

We have fit Eq. (1) to our experimental magnetoplasmon frequencies summarized in Fig. 6. We clearly see two distinct sets of modes denoted by 1 or 2. It is important to note that those combinations of absorptions are the only ones that can be fit with Eq. (1). The obtained parameters, namely the cyclotron masses and the screened plasma frequencies, are presented in Table I. Given the good quality of the fits, we can make two observations: (i) the values of plasma frequencies are close to those measured for a single crystal at $B = 0$ [18,21,22], and (ii) the temperature dependence of ω_+^1 is similar to that determined for monocrystal [23], which is expected as it comes from the variations of the total density when temperature changes. It appears that ω_- has no temperature dependence between 5.7 and 50 K, which is expected in low field (i.e., below the quantum limit) [9]. If we compare the very low field part

TABLE I. Fit parameters obtained with Eq. (1) at 5.7 and 50 K for each series of modes. Masses are in units of the mass of the electron, and optical modes are in units of cm^{-1}.

Temperature		Series 1	Series 2
5.7 K	$\omega_{p,h}$	115	139
	$\omega_{p,l}$	125	132
	$m_{c,h}$	0.275	0.148
	$m_{c,l}$	0.034	0.008
50 K	$\omega_{p,h}$	125	141
	$\omega_{p,l}$	127	140
	$m_{c,h}$	0.424	0.128
	$m_{c,l}$	0.039	0.008

of the fits of the magnetoplasmon resonances at 5.7 K with the resonance observed in microwave absorption obtained by Smith *et al.* [11] along the three main axes of the unit cell of bismuth, we can see that those measurements, performed with the Azbel'-Kaner method (**B//** surface of the sample, normal incidence of light), revealed oscillations of charge density for very similar values of magnetic fields.

V. CONCLUSION

In summary, we have measured the far-infrared reflectivity of polycrystalline bismuth in a magnetic field. We attribute to magnetoplasmon resonances the several features that we observed under a magnetic field, which become, in the low-field limit, optical and acoustic resonances of an electron-hole system. The use of a polycrystalline sample has helped us to observe experimentally the acoustic plasmon modes due to lowered translational symmetry. In the limit of zero field, however, the optical modes of these two series converge onto plasma frequencies measured in a monocrystal along the main optical axes. Our observation of well-defined resonances paves the way for optical spectroscopy research of materials for which only polycrystalline samples are available. Valuable information, at least about the temperature or magnetic-field dependence of the resonant frequencies, can be gained. The unique peculiarities of bismuth are probably related to the extreme anisotropy of its electronic properties, thus strongly anisotropic materials would be potential candidates for further studies.

ACKNOWLEDGMENTS

The authors thank Adrien Stucky, Damien Stricker, Michaël Tran, and Radovan Cerny for technical assistance, and we are grateful to Thierry Giamarchi for fruitful discussions. This work is supported by MaNEP and by the SNSF through Grant No. 200020-135085 and the National Center of Competence in Research (NCCR) "Materials with Novel Electronic Properties-MaNEP."

APPENDIX: STANDARD THEORY OF MAGNETOPLASMON

The collective mode (in which we are interested) is defined as a zero of a longitudinal dielectric function $\epsilon_{||}(q,\omega)$ of a material. An effective interaction in any material is a bare Coulomb interaction $V_0(q)$ divided by a tensor $\hat{\epsilon}(q,\omega)$, the $\epsilon_{||}(q,\omega)$ being its diagonal component. The dielectric function contains all screening processes and is built out of a series of particle-hole bubbles. The result of the simplest random phase (RPA) resummation of such scattering processes gives an effective interaction:

$$V_{\text{eff}}(q,\omega) = \frac{V_0(q)}{\epsilon_{||}(q,\omega)} = \frac{V_0(q)}{1 - V_0(q)\sum_\nu \Pi_\nu(q,\omega)}, \qquad \text{(A1)}$$

where the sum is taken over polarizabilities $\Pi_\nu(q,\omega)$ of all families $\nu = h,e1,e2,e3$ of carriers in bismuth. The denominator of Eq. (A1) defines $\epsilon_{||}(q,\omega)$. The polarizability $\Pi_\nu(q,\omega)$ is defined as a Fourier transform of a time-ordered correlation function of densities: $\Pi_\nu^{xx}(q,\tau) \equiv -\langle T_\tau \rho_\nu^x(q,\tau)\rho_\nu^x(-q,0)\rangle$ (where for once we put the space index to emphasize that we work with longitudinal polarization, with the electric field $\vec{E} \parallel x$). In the case of noninteracting fermions without magnetic field, the polarizability is given by the so called electron-hole (two-particle) propagator in the pocket ν:

$$\Pi_\nu^0(q,\omega) = \sum_{\vec{k}} \frac{f\left(\xi_k^\nu\right) - f\left(\xi_{k+q}^\nu\right)}{\omega + \xi_k^\nu - \xi_{k+q}^\nu + 0^+}, \qquad \text{(A2)}$$

where we did not include the spin index, as a summation over it is implicit (bismuth is a nonmagnetic material), and $f(\xi_k^\nu)$ is a Fermi-Dirac distribution. The masses enter our problem through *eigenenergies* $\xi_{\vec{k}}^\nu \sim \sum_{a,b,c} k_i^2/2m_i^\nu$ of carriers in each pocket ν. ($m_{a,b,c}$ are masses along the axis of ellipsoidal pocket ν. In Bi these masses are extremely anisotropic, and in each ellipsoid the main axes are oriented differently; see Fig. 1.) The sum in Eq. (A2) is known and leads to the Lindhard function. Equation (A2) is useful for us throughout the discussion; the principal Eq. (1) can be derived using $\Pi_\nu^0(q_x \to 0,\omega)$ (for a simplistic model of two spherical pockets and if the magnetic-field energy is included in the *eigenenergies*).

Magnetic field $\vec{B}$ (with certain orientation $\parallel z$ taken perpendicular to $\vec{E}$) enters via cyclotron mass to the eigenenergies ξ_k^ν and thus affects the polarizability, which is now $\Pi_\nu(q,\omega;\vec{B})$. The cyclotron mass depends on the cross section (in the plane x-y) of a given pocket of a Fermi surface, thus in the case of bismuth it is different for different carriers.

In a polycrystal, when the size of the grains is small, the formula Eq. (A2) is slightly modified: due to a finite size, the allowed values of momenta are quantized, and if carriers can propagate between grains, then we must allow for intergrain scattering, an effect that enters inside a bubble as a vertex correction. Moreover, some screening processes may take place in the neighboring grains, which inserts additional bubbles, with different masses, into the RPA series. This is how intergrain coupling enters into plasmon dispersion.

The density-density interactions that drive the (optical) plasmon instability are of long-range order. This is because screening is caused by plasmons themselves, so interactions are screened only for processes with energy lower than the frequency of collective excitations. The fact that the electron-electron interactions have a long-range character means that the density-density interactions dominate. Moreover, large anisotropy of a mass tensor implies that only a limited fraction of interfaces are transparent for the electron-hole waves (in fact, due to vertex corrections, also within Π_0 itself the low-angle scattering is preferable). In these circumstances, when we resort to pole expansion of $\epsilon_{||}$ in Eq. (A1), the quasiclassical approximation of coupled harmonic oscillators, used in Sec. IV, is applicable.

[1] Z. Zhu, B. Fauqué, Y. Fuseya, and K. Behnia, Phys. Rev. B **84**, 115137 (2011).
[2] W. J. de Haas and P. M. van Alphen, Proc. R. Acad. Sci. Amsterdam **33**, 1106 (1930).
[3] L. Shubnikov and W. Y. de Haas, Comm. Phys. Lab. Univ. Leiden 207a (1930).
[4] Y. Liu and R. E. Allen, Phys. Rev. B **52**, 1566 (1995).
[5] D. Hsieh, D. Qian, L. Wray, Y. Xia, Y. S. Hor, R. J. Cava, and M. Z. Hasan, Nature (London) **452**, 970 (2007).
[6] Z. Zhu, A. Collaudin, B. Fauqué, W. Kang, and K. Behnia, Nat. Phys. **8**, 89 (2011).
[7] L. Li, J. G. Checkelsky, Y. S. Hor, C. Uher, A. F. Hebard, R. J. Cava, and N. P. Ong, Science **321**, 547 (2008), http://www.sciencemag.org/content/321/5888/547.full.pdf.
[8] R. Tediosi, N. P. Armitage, E. Giannini, and D. van der Marel, Phys. Rev. Lett. **99**, 016406 (2007).
[9] P. Chudzinski and T. Giamarchi, Phys. Rev. B **84**, 125105 (2011).
[10] D. Pines and J. R. Schrieffer, Phys. Rev. **125**, 804 (1962).
[11] G. E. Smith, L. C. Hebel, and S. J. Buchsbaum, Phys. Rev. **129**, 154 (1963).
[12] N. D. Mermin, Ann. Phys. (N.Y.) **26**, 247 (1964).
[13] K. W. Chiu and J. J. Quinn, Phys. Rev. B **9**, 4724 (1974).
[14] H. Noto, J. Phys. Soc. Jpn. **36**, 1137 (1974).
[15] D.-W. Wang, S. Das Sarma, E. Demler, and B. I. Halperin, Phys. Rev. B **66**, 195334 (2002).
[16] J. Levallois, M. Tran, and A. B. Kuzmenko, Solid State Commun. **152**, 1294 (2012).
[17] R. E. Sherriff and R. P. Devaty, Phys. Rev. B **41**, 1340 (1990).
[18] W. S. Boyle, A. D. Brailsford, and J. K. Galt, Phys. Rev. **109**, 1396 (1958).
[19] S. Das Sarma, Phys. Rev. B **28**, 2240 (1983).
[20] J. Levallois, M. K. Tran, C. Uher, D. van der Marel, and A. B. Kuzmenko (unpublished).
[21] R. Tediosi, Ph.D. thesis, University of Geneva, 2008.
[22] A. D. LaForge, A. Frenzel, B. C. Pursley, T. Lin, X. Liu, J. Shi, and D. N. Basov, Phys. Rev. B **81**, 125120 (2010).
[23] N. P. Armitage, R. Tediosi, F. Lévy, E. Giannini, L. Forro, and D. van der Marel, Phys. Rev. Lett. **104**, 237401 (2010).